Molecular upconversion in water in heteropolynuclear supramolecular Tb/Yb assemblies

Aline Nonat,[a] Sylvana Bahamyirou,[a] Alexandre Lecointre,[a] Frédéric Przybilla,[b] Yves Mély,[b] Carlos Platas-Iglesias,[c] Franck Camerel,[d] Olivier Jeannin,[d] and Loïc J. Charbonnière*[a]

[a] Equipe de synthèse pour l'analyse (SynPA), Institut Pluridisciplinaire Hubert Curien (IPHC, UMR 7178), CNRS/Université de Strasbourg, ECPM, 25 rue Becquerel, 67087 Strasbourg Cedex, France. E-mail : l.charbonn@unistra.fr

[b] Laboratoire de Bioimagerie et Pathologies CNRS UMR 7021 Faculté de pharmacie CS60024 74, route du Rhin, 67401 Illkirch-Graffenstaden, France.

[c] React Group, Departamento de Química, Facultade de Ciencias & Centro de Investigacións Científicas Avanzadas (CICA), Universidade da Coruña, 15071 A Coruña, Spain.

[d] Université de Rennes, CNRS, ISCR - UMR 6226, F-35000 Rennes, France.

ABSTRACT: Piling up excited states to reach upconversion (UC) is severely restricted by vibrational quenching mechanisms, especially when one looks at discrete molecular entities in solution. By carefully controlling the supramolecular assembly processes resulting from the strong electrostatic interactions between negatively charged Yb complexes and Tb^{3+} cations in aqueous solutions, we engineered the formation of heteropolynuclear complexes of $[(YbL)_2Tb_x]$ compositions (x = 1 and 2). These edifices display a phenomenon of cooperative photosensitization UC with green emission of the Tb cations upon NIR excitation at 980 nm in the Yb absorption band. The photophysical properties of the complexes were carefully investigated by steady-state and time-resolved luminescence experiments in D_2O, allowing to quantify the impact of the composition and pD of the solution on the emission intensity, as well as clarifying the exact cooperative photosensitization upconversion mechanism. Using optimized conditions, the energy transfer UC process could be observed for the first time in non-deuterated water with discrete molecular compounds.

INTRODUCTION

The conversion of low energy photons into high energy ones, upconversion (UC), has been largely studied and applied for bulk solids[1,2] and more recently for nanoparticles.[3-5] However, the miniaturization of UC devices down to the molecular scale is still in its infancy, with only a handle of examples.[6-10] Considering the issues associated with reproducibility, toxicity[11] or particular side effects such as enhanced permeability and retention observed with nanoparticles in bioanalytical applications,[12] the development of controlled discrete molecular probes represents an interesting alternative to alleviate these issues.

However, observing UC at the molecular scale in solution is a particularly challenging task[13] as OH, NH and CH oscillators encountered in the ligand backbones or in the solvent molecules are strong non-radiative competitors.[14,15] They efficiently quench the intermediate excited states, especially in the Near-Infrared Region (NIR), before these later may be excited again to a higher emitting energy level. The main strategies developed to circumvent this drawback consist in: (i) protecting the cation with polydentate ligands fulfilling the first coordination sphere; (ii) deuteration[16] or replacement of the ligand C-H bonds by C-F ones;[17] and (iii) displacing the solvent molecules as far as possible from the NIR emitters by introduction of bulky substituents on the ligand.[18] The combination of these strategies has led to remarkable improvements of the luminescent properties of NIR complexes, especially in the case of Yb.[19] However, with a few exceptions,[20] these successes concern organic solvents and there remain many efforts to be done to achieve similar results in water and aqueous solutions. Despite these drawbacks, molecular UC can afford advantages over the solid state approach. Typical synthetic procedures for the preparation of bulk solids or nanoparticles require grinding, high temperatures or annealing procedures, which result in a random distribution of active centres in the matrices. However, it was noticed by Auzel and Goldner[21] that some synthetic procedures could lead to a "clustering effect" with chemical clusters of few Å in size, in which the ion-ion interactions are tremendously increased. Thus, a directed molecular or supramolecular approach allows for a better control of the distances and ordering of the active centres and their gathering at the Å range, which might improve UC and

partly counterbalance the drawbacks of quenching oscillators.

It has long been demonstrated that Energy Transfer Upconversion (ETU) is among the most efficient mechanism to observe the UC phenomenon, even in the cases of molecular systems.[22] The combination of one or more intermediate donor atoms (sensitizers) relaying energy to the emitting acceptor centre affords potential advantages in terms of efficiency. With its single $^2F_{7/2} \rightarrow {}^2F_{5/2}$ electronic transition at *ca* 980 nm, trivalent Yb is the element of choice to act as a sensitizer. This transition is high enough in energy to prevent full quenching of the excited state by water OH oscillators. Furthermore, the energy difference between the two ^2F Yb energy level matches those of different electronic transitions of numerous other trivalent lanthanides such as Er, Ho, Tm, Tb or Eu.

A particularly interesting case is that of the Yb/Tb sensitizer/acceptor pair. Although there is no electronic transition of Tb corresponding to the $^2F_{5/2}$ energy level of Yb, it has been observed that Yb can photosensitize Tb in solids through a mechanism of cooperative sensitization (Figure 1).[23] The simultaneous deactivation of two Yb centres is accompanied by energy transfer to the Tb atom which then emits in the visible region.

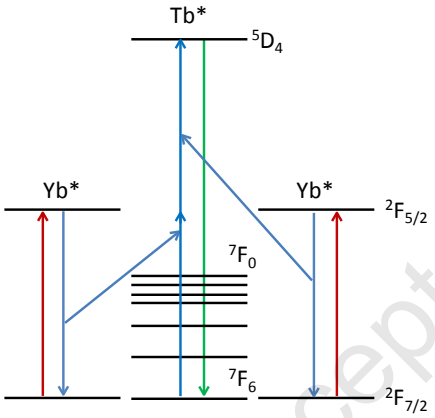

Figure 1. Principle of cooperative UC photosensitization of Tb by Yb.[23]

Alternatively, the UC mechanism leading to Tb emission upon Yb excitation was attributed in some instances to a mechanism involving ground state absorption (GSA) followed by excited state absorption (ESA). However, this mechanism holds for Yb/Tb pairs having very short intermetallic distances (3.89 Å for $Cs_3Tb_2Br_9$ doped with Yb).[24] Furthermore, it could only be observed at low temperatures, for which the phonon assistance to cooperative sensitization is no longer efficient.[25] The distinction between the two main mechanisms GSA/ESA or cooperative sensitization UC is generally made by pulsed excitation experiments, showing immediate increase of UC emission for ESA, but a slow rise of the UC emission intensity after pulsed excitation, due to the supplementary energy transfer step, for cooperative sensitization.[23]

Within the framework of our research on lanthanide coordination chemistry, we have recently developed a series of phosphonated ligands. Ligands containing phosphonate functions generally impart a larger thermodynamic stability to Ln complexes than their carboxylate counterparts.[26,27] Bulkier than carboxylates, phosphonates engender steric compression around the metal ion, which often results in a decrease of the coordination number (CN). This may lead to the removal of water molecules from the first coordination sphere of lanthanides as for the octadentate ligand 1,4,7,10-Tetraazacyclododecane-1,4,7,10-tetraacetic acid ligand (DOTA, CN = 9)[28] compared to 1,4,7,10-tetraazacyclododecane-1,4,7,10-tetrakis(methylenephosphonic acid) ligand (DOTP, CN = 8),[29] or for the heptadentate pyridine tetracarboxylate (CN = 9)[30] compared to its phosphonated analogue (CN = 8).[31] Finally, the negative charges of the phosphonate functions bring significant second sphere contributions to the relaxivity of Gd complexes,[32] which can become as important as the contribution of the first sphere.[33] Interestingly, the second sphere interactions of mononuclear phosphonated lanthanide complexes can be favourably mastered to construct higher order polynuclear[34,35] and heteropolynuclear[10] species.

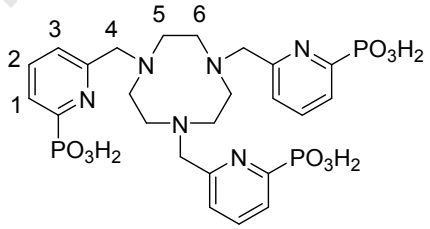

Scheme 1. Ligand L and the H atom numbering for NMR spectral assignment

Taking advantage of this principle, we here demonstrate that the mononuclear complex of L (Scheme 1) with Yb, noted (YbL) can form supramolecular species of formula $[(YbL)_2Tb_x]$ (x = 1 or 2) in the presence of Tb cations in aqueous solutions. In these adducts, NIR excitation of Yb at 980 nm resulted in a cooperative photosensitization of Tb with emission in the visible region. The assembly process was studied by a combination of various spectroscopic techniques and the resulting UC phenomenon was quantitatively and mechanistically investigated in D_2O. Taking advantage of the optimized conditions determined from D_2O, the UC conversion process evidenced in non-deuterated water for the first time from a molecular specie.

RESULTS AND DISCUSSION

Solid state and solution structure of the (YbL) complex. The (YbL) complex was prepared according to literature procedure.[34] Slow evaporation of an aqueous

solution of the (YbL) complex resulted in the formation of crystals suitable for X-ray crystal structure analysis (Figure 2).

The structure is composed of an Yb(III) cation embedded into the cavity formed by the 1,4,7-Triazacyclononane (tacn) ligand with the three pyridyl arms being wrapped around the cation. The Yb atom is nine coordinated with three nitrogen atoms from the tacn macrocycle, the three pyridyl nitrogen atoms and three oxygen atoms from the phosphonic acid moieties. The three strands are wrapped around the metal providing a pseudo-C_3 axis passing through the Yb atom and perpendicular to the plane formed by the nitrogen atoms of the tacn cycle. The wrapping led to the formation of Δ and Λ isomers. Both isomers are present in the centrosymmetric crystal structure. Using the SHAPE program,[36] the geometry of the first coordination sphere of Yb was shown to be very close to a spherical trigonal prism, which is characterized by identical center-to-vertex distances.[37] The Yb atom is almost contained in the plane formed by the three nitrogen atoms of the pyridyl rings with a slight deviation from the mean plane of 0.003 Å. The three phosphonate functions are monoprotonated, allowing a compensation of the overall charge and the formation of a neutral complex.

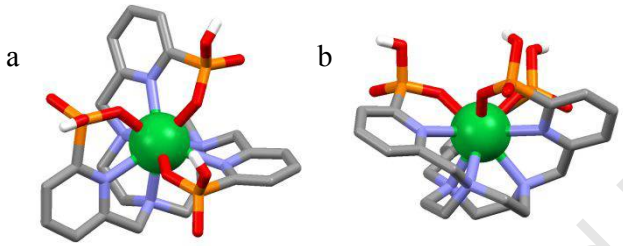

Figure 2. X-Ray crystal structure of the (YbL) complex viewed along (a) and perpendicularly (b) to the pseudo-C_3 axis.

The structure of the Yb complex in solution was further studied by analyzing the ^{1}H paramagnetic lanthanide induced shifts (LIS).[38] The ^{1}H NMR spectrum presents the 9 paramagnetically-shifted signals expected for an effective C_3 symmetry in D_2O, observed in the range 24 to -18 ppm (Figure S1 and Table S1, Supp. Inf.). The attribution of the proton signals was achieved by linewidth analysis, as the broadening of the ^{1}H signals induced by the paramagnetism of the metal ion is proportional to $1/r^6$, where r is the distance between the observed nucleus and the paramagnetic ion.[39] Thus, the ^{1}H NMR signals of axial protons (r(Yb···H) = 3.4-4.2 Å) are considerably broader than those of the equatorial resonances (r(Yb···H) = 4.4-4.5 Å). The paramagnetic shifts induced by Yb^{3+} are dominated by the pseudo-contact (PC) mechanism, which in the case of axially symmetric systems can be expressed as:[38]

$$\delta^{PC} = D_1 \frac{(3cos^2\theta - 1)}{r^3} \qquad (1)$$

In (1), r is the distance between the paramagnetic ion and the observed nucleus, while θ is the angle defined by the Yb-H vector and the principal magnetic axis of the system and D_1 is a proportionality constant related to the axial component of the magnetic susceptibility tensor.

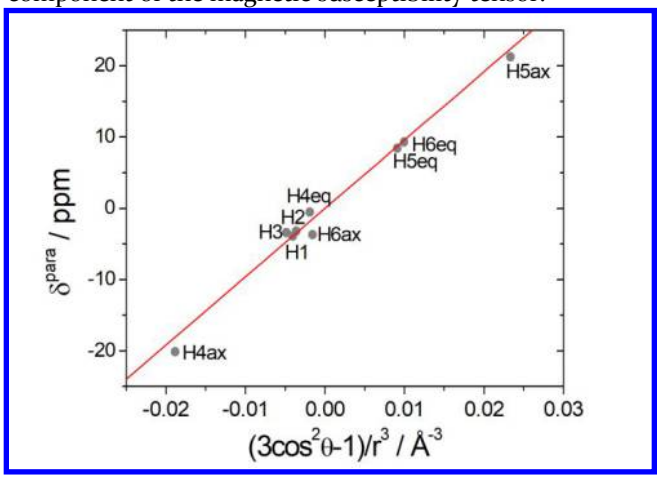

Figure 3. Plot of the paramagnetic shifts versus the geometric factors for the different proton nuclei of the Yb^{3+} complex. The red line corresponds to the linear fit of the data (See Scheme 1 for H atom labeling).

The paramagnetic shifts (δ^{para}) observed for the Yb^{3+} complex were analyzed with Eq (1) using the chemical shifts observed for the Lu^{3+} diamagnetic analogue to estimate the diamagnetic contribution (δ^{dia}) to the observed chemical shifts (δ^{obs}):

$$\delta^{para} \approx \delta^{PC} = \delta^{obs} - \delta^{dia} \qquad (2)$$

The geometric terms $(3\cos^2\theta - 1)/r^3$ of the different nuclei of the Yb^{3+} complex were estimated from both the X-ray structure and density functional theory (DFT) calculations (Table S1 and S2).[40] The structure obtained by DFT is very similar to the X-ray structure described above.

Plots of the observed paramagnetic shifts versus the geometric factors provide straight lines passing through the origin. The linear correlation obtained from this analysis is better when using the DFT geometry (R^2 > 0.994) than the X-ray structure (R^2 > 0.988), indicating that DFT provides a better description of the structure of the complex in solution. Nevertheless, the Yb^{3+} complex retains the axially symmetric C_3 structure observed in the solid state upon dissolution in water. The slope of the linear plot provides D_1 = 960 ppm Å^3 (Figure 3). The value of D_1 obtained for this complex is ca. 3 times smaller than those reported for cyclen-based complexes showing capped square antiprismatic coordination,[41,42] and about 56% of the value reported for the tris(dipicolinate) Yb^{3+} complex (D_1 ~ 1700 ppm Å^3).[43] This points to a rather small anisotropy of the $^2F_{7/2}$ ground state in the Yb^{3+} complex investigated here.[44]

The electronic absorption spectrum of the (YbL) complex in D_2O (Figure S2) in the NIR region displays a broad absorption band centred around 980 nm which corresponds to the $^2F_{7/2} \rightarrow {}^2F_{5/2}$ Yb transition. The radiative lifetime of Yb in the complex in D_2O, τ_{rad}, was calculated from this spectrum using the methodology developed by Werts and coworkers[45] (see Supplementary information

for full details). A radiative lifetime of 1.36 ms was determined, which provides a metal centred luminescence efficiency of 0.75 % using equation (3):

$$\phi_{Yb} = \frac{\tau_{obs}}{\tau_{rad}} \qquad (3)$$

Where τ_{obs} is the measured luminescence lifetime of the complex in D_2O (10.2 µs [35]). It is to be noticed that a long Yb excited state lifetime is of critical importance for the observation of UC in the system. As two excited Yb atoms have to transfer their energy to Tb, the probability of such a transfer is strongly depending on the probability to have excited pairs, hence on the excited state lifetime of the Yb centers.

Cooperative UC sensitization in D_2O. We have recently shown[35] that the addition of excess Ln^{3+} cations to solutions of the [LnL] complexes led to the formation of two new species with $[(LnL)_2Ln]$ and $[(LnL)_2Ln_2]$ compositions. These polynuclear complexes were found to be inert, so that exchange of one Ln chelated inside the cavity of the ligand by a second Ln' cation added into the solution does not occur at neutral pH. From this observation, we hypothesized that addition of up to one equivalent of Tb cations to a solution of the [YbL] complex would lead to the formation of the heteropolynuclear $[(YbL)_2Tb]$ and $[(YbL)_2Tb_2]$ complexes, with potentially interesting properties in terms of cooperative UC photosensitization, according to:

$$2\,(YbL) \xrightarrow{Tb^{3+}} [(YbL)_2Tb] \xrightarrow{Tb^{3+}} [(YbL)_2Tb_2]$$

To further confirm the absence of scrambling into the solution, ^1H- and ^{31}P-NMR experiments were run using a solution of [YbL] in D_2O (pD = 7.7), to which 0, 0.5 and 1.0 equivalents of $LuCl_3$ were added. A second experiment consisted in the addition of one equivalent of $YbCl_3$ to a solution of [LuL] (pD = 7.9). The spectra measured immediately after addition of the salt or after 7 days at 80°C are identical. However the two experiments provided very different spectra (Figure S9), showing smaller paramagnetic shifts when the paramagnetic Yb atom was added to the [LuL] complex. These results confirmed the lack of scrambling in these conditions. Additionally, ^1H-NMR spectra of solutions of 0.5 and 1.0 equivalent of $TbCl_3$ to a D2O solution of the [YbL] complex were even less informative with the concomitant effects of the paramagnetic contributions of Tb and Yb (Figure S10 and S11). Finally, a potential scrambling of the two kinds of lanthanide inside/outside the ligands was checked by luminescence spectroscopy experiments in which 0.5 and 1.0 equivalent of $EuCl_3$ were added to solutions of [YbL] in water. Excitation into the ligand absorption band (267 nm) revealed an Eu centred emission, as a result of the spatial proximity of Eu and the ligands in the polynuclear assemblies. However, determination of the luminescence lifetimes were particularly informative (Figure S12). The decay of the solution at 0.5 eq., associated to the formation of the $[(YbL)_2Eu]$ as the main species with our model, was satisfactorily fitted with a mono-exponential decay with a lifetime of 655 µs. The decay of the equimolar solution, associated to the formation of $[(YbL)_2Eu_2]$ as the main species, was fitted with a bi-exponential decay with lifetimes of 257 µs (44%) and 659 µs (56%). All the lifetimes determined are far below the value expected for an Eu cation embedded into the cavity of the ligand (1.26 ms),[35] a good evidence of the lack of scrambling, at least on the timescale of the experiments at room temperature and also after four days of heating at 70°C after which no significant changes could be observed.

To confirm our hypothesis, a solution of (YbL) in D_2O was titrated by increasing amounts of a solution of $TbCl_3.6H_2O$ in D_2O. After each addition of aliquots of Tb salts, the pD of the solution was raised to 7.0 and the emission spectrum of the solution was recorded in the visible region upon 980 nm excitation. A 850 nm high-pass filter was placed between the excitation source and the sample to remove possible second order artefacts. Figure 4 represents the typical emission spectrum observed upon addition of 1.0 equivalent of $TbCl_3.6H_2O$, while the inset shows the evolution of the emitted signal as a function of the number of equivalents of Tb added to the (YbL) solution.

From Figure 4, it clearly appears that the emission spectrum results from the $^5D_4 \rightarrow {}^7F_J$ (J = 6 to 3) transitions of Tb.[46] The decrease of the intensity above one equivalent was ascribed to the formation of a precipitate, as previously observed in the case of the NMR titration of L by Lu at mM concentrations.[35] In order to evidence the importance of the Yb complex in the UC process, and to exclude a possible sensitization of Tb by a non-linear excitation of the ligand, a similar titration was performed using the optically silent [LuL] complex in place of [YbL]. Excitation at 980 nm resulted in the total absence of Tb emission during the titration. To further characterize the UC sensitization of Tb, the intensity of the Tb emission was recorded as a function of the excitation power density.

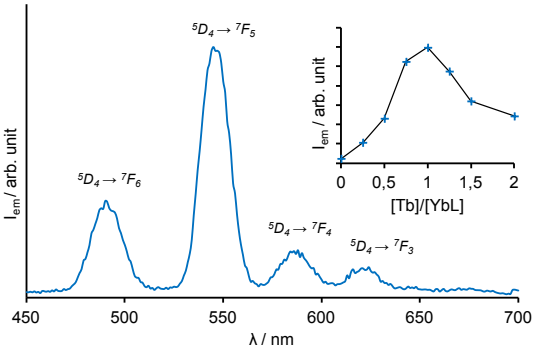

Figure 4. Emission spectrum measured upon addition of 1.0 equivalent of $TbCl_3.6H_2O$ to a 1.25 mM solution of (YbL) in D_2O at pD 7.1 (λ_{exc} = 980 nm, P_{980} = 1.08 W). Inset: Evolution of the emission intensity as a function of the [Tb]/[YbL] ratio.

The corresponding Log-Log plot shown in Figure 5 clearly evidences a slope of almost 2, representative of the

quadratic dependence of a two photon excitation mechanism.[47]

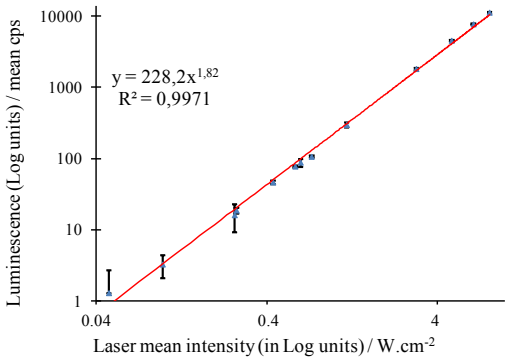

Figure 5. Log-Log plot of the Tb emitted intensity at 545 nm as a function of the excitation intensity of the 975 nm laser for a 1.53 mM solution of (YbL) in D_2O containing 0.5 equivalent of $TbCl_3.6H_2O$ at pD = 9.2.

Interestingly, the pD of the solution appeared to be a very important factor and an order of magnitude in the emission intensity could be gained by adjusting the pD of the solution. Importantly, the adjustment must be done only after the addition of the Tb salts, to avoid the formation of insoluble Tb hydroxy species. The best pD range was found to be close to 9.15 (Figure S3).

Determination of the UC luminescence quantum yield in D_2O. Full experimental details for the calculation of the UC quantum yield, QY_{UC}, can be found in the Supplementary Information section. It consisted in using the basic definition of the luminescence quantum yield as being the ratio of the number of emitted photons to the number of absorbed photons, while comparing the emitted signal (Figure S4) to that of a Tb reference (Figure S5).[48] By applying this methodology, QY_{UC} was determined to be 1.4×10^{-8} with a large relative uncertainty of ± 20%. Accordingly, this QY_{UC} value should better be considered as an order of magnitude rather than an absolute figure.

Mechanistic study of the UC process in D_2O. Literature data on Tb/Yb codoped systems describe different mechanisms for the observed UC emission of Tb. A first possible mechanism consists in the successive excitation of two Yb atoms, followed by their simultaneous energy transfer to populate the Tb excited state, as represented in Figure 1.[23] This mechanism is related to the GSA/ETU mechanism observed in conventional UC probes. A fingerprint of this mechanism is a slow rise of the UC emission before decay after a pulsed excitation.

A second mechanism refers to Yb-Tb exchange coupled dimers,[24] in which the Ln atoms are close enough in space to allow some exchange interactions. This mechanism is then described by:

$$\left|Yb(^2F_{7/2}),Tb(^7F_6)\right\rangle + h\nu \rightarrow \left|Yb(^2F_{5/2}),Tb(^7F_6)\right\rangle + h\nu \rightarrow \left|Yb(^2F_{5/2}),Tb(^5D_4)\right\rangle$$

For this mechanism, relevant to the principle of GSA/ESA mechanism of conventional UC processes, the basic features are the observation of an immediate decay of the UC efficiency after short-pulsed excitation, and the appearance in the UC spectrum of transitions which do not match the emission spectrum of the emitting atom, *i.e.* Tb, as a result of admixture with the Stark levels of Yb in the Yb/Tb dimers.[24]

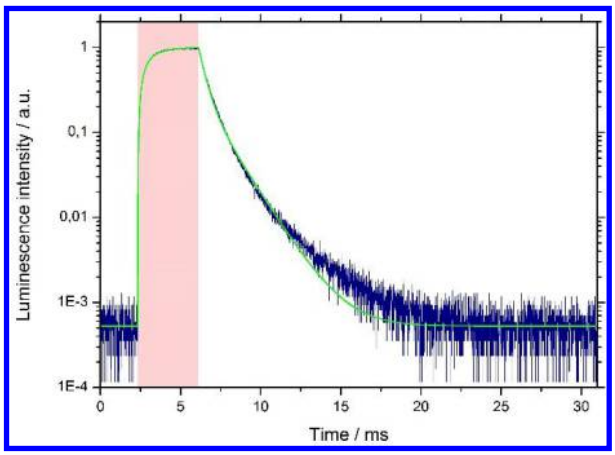

Figure 6. Evolution with time of the Tb centred UC emission intensity at 550 nm (in blue) upon time gated excitation at 975 nm (schematized in pink) for a 1.53 mM solution of [YbL] in D_2O (pD = 9.2) containing 0.5 equivalent of $TbCl_3.6H_2O$. The green curve represents the fit of the data according to a two Tb sites model (see text).

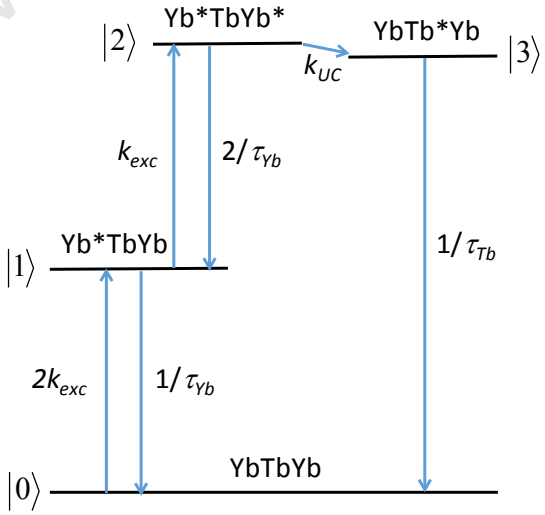

Figure 7. Energy level diagram of the cooperative UC photosensitization of Tb in the [(YbL)2Tb] supramolecular complex.

To get insights into the mechanism, we performed time-resolved luminescence measurements in which the continuous wave output of a 975 nm laser diode was electronically modulated to generate excitation pulses with a square temporal profile. Single photon events are detected at 550 nm using the time-correlated single photon

counting approach. Full experimental details can be found in the experimental section, while the setup is schematized in the supplementary information section (Figure S6). A representative photon distribution over time is given in Figure 6.

As can be observed in Figure 6, the rise of the UC emission intensity is quite long, requiring few ms before it reaches steady-state. This slow rise is typical of a slow kinetic step related to the energy transfer during the cooperative energy transfer UC process.[23] Considering the energy level diagram for the cooperative photosensitization UC process (Figure 7), and regarding a similar model proposed for ETU in supramolecular complexes,[49] a mathematical model was developed to fit the measured evolution of the luminescence intensity with time. The evolution of the populations of the different states can be calculated using the following matrix description:

$$\frac{d}{dt}\begin{pmatrix}|0\rangle\\|1\rangle\\|2\rangle\\|3\rangle\end{pmatrix}=\begin{pmatrix}-2k_{exc} & 1/\tau_{Yb} & 0 & 1/\tau_{Tb}\\ 2k_{exc} & -1/\tau_{Yb}-k_{exc} & 2/\tau_{Yb} & 0\\ 0 & k_{exc} & -2/\tau_{Yb}-k_{UC} & 0\\ 0 & 0 & k_{UC} & -1/\tau_{Tb}\end{pmatrix}\times\begin{pmatrix}|0\rangle\\|1\rangle\\|2\rangle\\|3\rangle\end{pmatrix}$$

Where k_{exc} is the pumping rate constant, τ_{Yb}, is the excited state lifetime of Yb in the absence of Tb (10.2 µs),[35] τ_{Tb}, the excited state lifetime of Tb (fitted in the process) and k_{UC}, the rate of the energy transfer step (fitted). In this model, it is assumed that the absorption properties of the [YbL] unit are the same for all entities ([YbL] and [$(YbL)_2Tb$]). The pumping rate constant was determined using the relationship:[21]

$$k_{exc}=\frac{\lambda_P}{hc}P\sigma_{Yb}^{0\rightarrow1} \qquad (4)$$

with λ_P is the pumping wavelength, h, the Planck's constant, c the vacuum speed of light, P the incident pump intensity and $\sigma_{Yb}^{0\rightarrow1}$ the absorption cross section (in cm^2/molec) of the Yb $^2F_{7/2} \rightarrow {}^2F_{5/2}$ transition obtained from the electronic absorption spectrum (Figure S2).

While fitting the data, it soon appeared that such a simplified model did not allow to properly describe the observed evolution of the emission intensity. In particular, the decay part shows a bi-exponential behaviour, pointing to the emission of two distinct Tb sites. This observation can be related to the presence of both the [$(YbL)_2Tb$] and [$(YbL)_2Tb_2$] species being present in solution even at only 0.5 equivalent of added Tb. It was thus necessary to revise the model and to include the two heteropolynuclear species. This required the introduction of four new variable parameters in the fitting: the two luminescence lifetimes of the Tb atoms of the [$(YbL)_2Tb_2$] complex, and the two UC rate constants associated to the populations of these two new Tb sites. A fitting with six variables being over-dimensioned in respect to our data, we hypothesized that the introduction of the second Tb atom does only marginally change the structural properties of the [$(YbL)_2Tb$] precursor. Consequently, the UC rate constant and luminescence lifetime of the Tb atom in [$(YbL)_2Tb$] were assumed to be the same as that of one of the Tb atom of the [$(YbL)_2Tb_2$] species, reducing the number of variable parameters to four: the two Tb luminescence lifetimes and the two UC rate constants. This model is illustrated by the energy level diagram represented in Figure S7 and its matrix description in Figure S8.

The data could well be fitted with this new model as can be seen in Figure 6 (green curve). From this fit, Tb luminescence lifetimes of 0.42 ± 0.05 ms and 1.45 ± 0.05 ms were determined with associated UC rate constants of 2330 ± 30 and 278 ± 4 s^{-1} respectively. The same analysis was performed on an equimolar solution of [YbL] and Tb, and the corresponding figure with the fitted data is presented in Figure S13. The values obtained for the UC rate constants are in agreement with the 2000 s^{-1} value determined by Güdel and coworkers for single crystals of $SrCl_2$ doped with Yb and Tb at 1%.[23] However, great care should be taken with the comparison between our system in solution and the solid state data of Güdel et al. (room temperature and a laser peak power of 81 $W.mm^{-2}$ in our case and 100 K and 10^7 $W.mm^{-2}$ for the work of Güdel). Additionally, one should keep in mind that our treatment, as that of Hauser and coworkers,[49] is related to intramolecular processes, in contrast to the intermolecular ones in the approach of Güdel.[23] Interestingly, it is to be noticed that the faster energy transfer process is related to the shorter lived Tb excited state. Taking into account that this kind of cooperative sensitization is phonon assisted, one may expect the O-D oscillators of the solvent molecules to play a role in the phonon assistance, especially for the most solvated Tb cation, *i.e.* the one with the shorter excited state lifetime.

The efficiency of the UC process, η_{UC}, can be calculated using the relationship:

$$\eta_{UC}=\frac{\sum k_{UC}}{\sum k_{UC}+k_r+k_{nr}} \qquad (5)$$

where k_{UC} represents the UC energy transfer rate. The radiative rate constant k_r of the Yb complexes is the inverse of τ_r (1.36 ms, *vide supra*), that is 735 s^{-1}, while the non radiative rate constant k_{nr} can be obtained by:

$$\phi_{Yb}=\frac{k_r}{k_r+k_{nr}} \qquad (6)$$

ϕ_{Yb} being the Yb centred luminescence quantum yield (0.75 %, *vide supra*), giving a value of 97300 s^{-1} for k_{nr}. By this approach, the UC efficiency was calculated to be 2.6 % in our conditions. Alternatively, η_{UC} can be derived independently from the measurements of the Yb centred luminescence lifetimes in the absence (τ_{obsYb} = 11.4 µs at pD = 7.2) and in the presence (τ_{YbTb} = 11.2 µs at pD 7.1) of 0.5 equivalent of Tb using:

$$\eta_{UC} = 1 - \frac{\tau_{YbTb}}{\tau_{Yb}} \qquad (7)$$

This approach yields a value of 2.4 %, in excellent agreement with that obtained from equation (5).

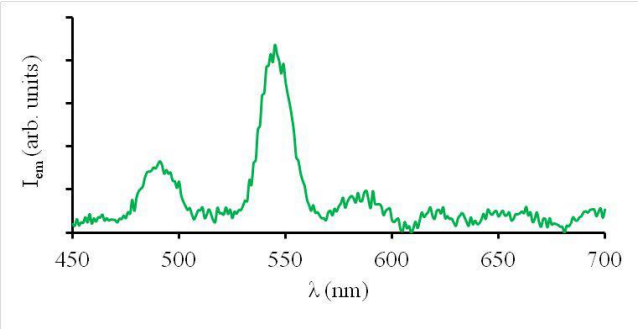

Figure 8. UC emission spectrum of an 11 mM solution of [YbL] in the presence of one equivalent of $TbCl_3.6H_2O$ upon excitation at 980 nm (P_{980} = 1.08 W).

UC in water. Considering the success obtained in observing UC in D_2O with our system, we turned our attention towards the possibility of observing UC in non-deuterated water. Assuming that the rate of the UC energy transfer step is not perturbed by the change from D_2O to H_2O (which may not be fully true, when considering the likely assistance of phonons in the process), the efficiency of the phenomenon is thought to be related to the square of the probability of Yb to be in the excited state, itself related to the squared value of the ratio of the Yb excited state lifetimes in the two solvents. For a same set of concentrations and technical parameters (slits, excitation power,...) the UC emitted intensity in H_2O should be related to that in D_2O divided by $(\tau_{YbD_2O}/\tau_{YbH_2O})^2$ = $(10.2/2.8)^2$ = 13.0. Additionally, the change from D_2O to water will result in a decrease of the Tb emission intensity due to additional vibrational relaxation. Considering the long lifetime of 1.46 ms obtained by the fitting process and a hydration number of 2 to 5 water molecules, application of Beeby's equation[14] showed that the decreased lifetime of Tb would result in a supplementary 1.5 to 3-fold decrease in the UC intensity in water. Thus, a *ca* ten-fold increase of the concentration associated to a longer accumulation time should allow for observing UC in water. The experiment was run on an 11 mM solution of [YbL] containing one equivalent of $TbCl_3.6H_2O$ and 120 scans were accumulated (six times more than for D_2O experiments, Figure 8).

As can be seen in Figure 8, the cooperative UC photosensitisation of Tb by Yb can also be observed in pure water, affording the first example of molecular UC in water at room temperature. Noteworthy, this result was obtained with a non-deuterated ligand, the synthesis of which being easily accessible. This observation paves the way to further improvements, potentially leading to a brand new family of luminescent tags based on molecular UC devices.

EXPERIMENTAL SECTION

Spectroscopy. Spectroscopic measurements were performed with 10×10 mm² quartz suprasil certified cells (Helma Analytics). UV/Vis absorption spectra were recorded on a Perkin-Elmer lambda 950 spectrometer. Steady-state emission spectra were recorded on an Edinburgh Instrument FLP920 spectrometer working with a continuous 450W Xe Lamp and a red sensitive R928 photomultiplier from Hamamatsu in Peltier housing for visible detection (230 to 900 nm) or a Hamamatsu R5509-72 photomultiplier for the Vis-NIR part. All spectra were corrected for the instrumental functions. For emission spectra upon UV excitation (Figure S4 and S5), a 399 nm cutoff filter was used to eliminate second-order artifacts. Phosphorescence lifetimes were measured on the same instrument working in the Multi Channel Spectroscopy (MCS) mode, using a Xenon flash lamp as the excitation source. For short µs lifetimes, the intensity decay was corrected from the lamp intensity decay profile using a scattering solution of Ludox in water. Steady-state upconversion emission spectra were recorded on the FLP920 spectrometer using a 980 nm LED from Edinburgh Instrument with a 850 nm high pass filter between the source and the sample to remove any potential visible excitation. The power of the LED was calibrated using a FieldMate power meter from Coherent Technology. Unless otherwise stated, the spectra were recorded using the Peltier cooled R928 photomultiplier from Hamamatsu, using fully opened emission slit width (20 nm), by accumulation of 20 spectra at 1 point/nm, with a dwell time of 0.1 s per nm.

Power dependent steady-state and time-resolved UC luminescence measurements were performed in quartz cuvettes (Hellma QS Semi-Micro Cells). The continuous-wave laser beam (λ = 975 nm) of a single mode fiber coupled laser diode was collimated (Thorlabs, TC12APC-980) and focused in the cuvette by a +100 mm focal length lens. From the measured beam waist radius (w = 30.6 µm), we estimated the average excitation intensity in the beam waist to be 8.1 kW/cm² at maximum laser power. The emission of the sample was collected by a 10x / 0.25 numerical aperture objective and focused on an avalanche photodiode (Excelitas, SPCM-AQRH-16). The scattered laser light was removed by a low pass filter (Chroma, ET750-SP-2P) and a band pass filter (Semrock, FF01-550/88-25). In the case of the steady-state measurements (emitted intensity as a function of excitation intensity) the output power of the laser was adjusted electronically (by varying the current intensity sent to the diode) and optically by using neutral density filters (Thorlabs) and systematically measured by a power meter (Newport, 1917R and Ophir, 30A-BB-18). The signal of the photodiode was collected by a computer equipped with a multifunction input/output card (National Instruments multifunction board, PCIe 6711). During time-resolved measurements, the laser output was modulated electronically at 32 Hz with a 12% duty cycle square waveform by a multifunction

input/output card (National Instruments multifunction board, PCIe 6361). The single photon events detected by the photodiode and the synchronization signal of the laser were recorded by a time-correlated single photon counting board (Becker-Hickl, SPC-830). The software SPCM 9.75 (Becker-Hickl) was used to both record the data and build the photon distribution over time. Experimental luminescence decays were fitted by using the coupled differential rate equations model discussed in main text in Matlab 2017b. A representation of the setup is schematized in Figure S6 (Supp. Inf.).

X-ray crystal structure of the (YbL) complex. Data were collected on a D8 VENTURE Bruker AXS diffractometer operating with graphite-monochromated Mo-*Kα* radiation (λ = 0.71073 Å). Two twin components were found using the CELL_NOW program as implemented in the APEXIII program suite. The structures was solved by direct methods using the *SIR92* program[50] and then refined with full-matrix least-square methods based on F^2 (*SHELXL-2014/7*)[51] with the aid of the WINGX program.[52] All non-hydrogen atoms were refined with anisotropic atomic displacement parameters. The H atoms of phosphonate groups have been found in the electron density maps and refined as idealized hydroxyl group with torsion from electron density (AFIX 147 instruction), H atoms of water molecules were not clearly identified in the electron density maps and have been omitted in the refinement, other H atoms were finally included in their calculated positions. Crystallographic data on X-ray data collection and structure refinements are given in Table S2-S6. Crystallographic data for structural analysis of the Yb complex has been deposited with the Cambridge Crystallographic Data Centre under CCDC 1589358. Copies of this information is available free of charge from the Web site (www.ccdc.cam.ac.uk).

DFT calculations. Following our previous work,[53] DFT calculations were performed with the hybrid meta-GGA TPSSh functional[54] in conjunction with a large-core quasirelativistic effective core potential (ECP) and the related (7s6p5d)/[5s4p3d]-GTO basis set or Yb,[55] and the standard 6-31G(d,p) basis set for C, H, N, O and P. Bulk water solvent effects were considered with the integral equation formalism of the polarized continuum model (IEFPCM).[56]

CONCLUSION

The strong kinetic and thermodynamic stability of the Ln complexes of ligand L associated to their large negative charges were advantageously used to form the heteropolynuclear $[(YbL)_2Tb]$ and $[(YbL)_2Tb_2]$ complexes in aqueous solutions. NIR excitation of the Yb atom in these heteronuclear edifices led to the observation of a cooperative photosensitization UC of Tb with emission in the visible domain. Time-resolved excitation experiments allowed to calculate the UC rate constants in the supramolecular adducts and to estimate a 2.6% efficiency of the UC step, that was confirmed by the decrease of Yb excited state lifetime in the presence of Tb. The overall efficiency of the UC process was found to be rather low in D_2O (1.4×10^{-8}), but sufficient to envisage its observation in non-deuterated water. Hence, for the first time, this cooperative photosensitization UC could be observed at the molecular scale in an aqueous solution at room temperature. Careful analysis of the parameters that control the UC efficiency suggests that engineering of improved supramolecular edifices will allow additional optimizations, so that the development of UC molecular probes for applications in bio-analytical technologies may be envisaged.

ASSOCIATED CONTENT

Supporting Information. ^{1}H-NMR spectrum of [YbL] in D_2O in presence of 0, 0.5 and 1 equivalent of $LuCl_3$ and $TbCl_3$^{1}H-NMR spectrum of [LuL] in D_2O in presence of 0 and 1 equivalent of $YbCl_3$, Electronic absorption spectrum of [YbL] in D_2O in the NIR region, Tb emitted intensity as a function of the pD, Experimental setup used for the time-resolved UC emission intensity measurements (4 Figures), Full experimental Procedures for the calculation of the radiative lifetime of Yb and the UC quantum yield, Crystallographic data for the structure of the Yb complex (5 Tables) geometric factors for the calculations of ^{1}H-NMR chemical shifts of the [YbL] complex (2 Tables), and Luminescence decay profiles of Eu recorded for two solutions of [YbL] in presence of 0.5 and 1 equivalent of $EuCl_3$ in water can be find in the supporting information section. This material is available free of charge via the Internet at http://pubs.acs.org.

AUTHOR INFORMATION

Corresponding Author

* l.charbonn@unistra.fr

ACKNOWLEDGMENT

Doctor Robert Pansu (Ecole Normal Supérieure de Cachan, France) is gratefully acknowledged for his advices and fruitful discussions concerning the determination of the luminescence UC QY. C. P.-I. thanks Centro de Supercomputación de Galicia for providing the computer facilities.

REFERENCES

(1) Auzel, F. Upconversion and anti-Stokes processes with f and d Ions in solids. *Chem. Rev.* **2004**, *104*, 139.

(2) Gamelin, D.R.; Güdel, H.U. Design of luminescent inorganic materials: new photophysical processes studied by optical spectroscopy. *Acc. Chem. Res.* **2000**, *33*, 235.

(3) Chen, G.; Qiu, H.; Prasad, P.N.; Chen, X. Upconversion nanoparticles : design, nanochemistry, and applications in theranostics. *Chem. Rev.* **2014**, *114*, 5161.

(4) Haase, M.; Schäfer, H. Upconverting nanoparticles. *Angew. Chem. Int. Ed.* **2011**, 50, 5808.

(5) Zheng, W.; Huang, P.; Tu, D.; Ma, E.; Zhu, H.; Chen, X. Lanthanide-doped upconversion nano-bioprobes: electronic

structures, optical properties, and biodetection. *Chem. Soc. Rev.* **2015**, *44*, 1379.

(6) Suffren, Y.; Golesorkhi, B.; Zare, D.; Guénée, L.; Nozary, H.; Eliseeva, S. V.; Petoud, S.; Hauser, A.; Piguet, C. Taming Lanthanide-Centered Upconversion at the Molecular Level. *Inorg. Chem.* **2016**, 55, 9964.

(7) Aboshyan-Sorgho, L.; Besnard, C.; Pattison, P.; Kittilstved, K.R.; Aebischer, A.; Bünzli, J.-C.G.; Hauser, A.; Piguet, C. Near infrared to visible light upconversion in a molecular trinuclear d-f-d complex. *Angew. Chem. Int. Ed.* **2011**, *50*, 4108.

(8) Hyppänen, I.; Lahtinen, S.; Ääritalo, T.; Mäkelä, J.; Kankare, J.; Soukka, T. Photon upconversion in a molecular lanthanide complex in anhydrous solution at room temperature. *ACS Photonics* **2014**, *1*, 394.

(9) Nonat, A.; Chan, C.F.; Liu, T.; Platas-Iglesias, C.; Wong, K.-L.; Charbonnière, L.J. Room temperature molecular up conversion in solution. *Nature Commun.* **2016**, *7*, 11978.

(10) Souri, N.; Tian, P.; Platas-Iglesias, C.; Chafaa, S.; Wong, K.L.; Nonat, A.; Charbonnière, L.J. Upconverted photosensitization of Tb visible emission by NIR Yb excitation in descrete supramolecular heteropolynuclear complexes. *J. Am. Chem. Soc.* **2017**, 139, 1456.

(11) Gnach, A.; Lipinski, T.; Bednarkiewicz, A.; Rybka, J.; Capobianco, J.A. Upconverting nanoparticles : assessing the toxicity. *Chem. Soc. Rev.* **2015**, *44*, 1561.

(12) Maeda, H. Tumor-selective delivery of macromolecular drugs via the EPR effect: Background and future prospects. *Bioconjugate Chem.* **2010**, *21*, 797.

(13) Charbonnière, L.J. Bringing upconversion down to the molecular scale. *Dalton Trans.* **2018**, *47*, 8566.

(14) Beeby, A.; Clarkson, I. M.; Dickins, R. S.; Faulkner, S.; Parker, D.; Royle, L.; de Sousa, A. S.; Williams, J. A. G.; Woods, M. Non-radiative deactivation of the excited states of europium, terbium and ytterbium complexes by proximate energy-matched OH, NH and CH oscillators: an improved luminescence method for establishing solution hydration states. *J. Chem. Soc. Perkin Trans 2*, **1999**, 493.

(15) Horrocks, W. D. W. Jr; Sudnick, D. Lanthanide ion probes of structure in biology. Laser-induced luminescence decay constants provide a direct measure of the number of metal-coordinated water molecules. *J. Am. Chem. Soc.*, **1979**, *101*, 334.

(16) Bischof, C.; Wahsner, J.; Scholten, J.; Trosien, S.; Seitz, M. Quantification of C–H quenching in near-IR luminescent ytterbium and neodymium cryptates. *J. Am. Chem. Soc.* **2010**, *132*, 14334.

(17) Ning, Y.; Tang, J.; Liu, Y.-W.; Jing, J.; Sun, Y.; Zhang, J.-L. Highly luminescent, biocompatible ytterbium(III)

complexes as near-infrared fluorophores for living cell imaging. *Chem. Sci.* **2018**, *9*, 3742.

(18) Hu, J.-Y.; Ning, Y.; Meng, Y.-S.; Zhang, J.; Wu, Z.-Y.; Gao, S.; Zhang, J.-L. Highly near-IR emissive ytterbium(iii) complexes with unprecedented quantum yields. *Chem. Sci.* **2017**, *8*, 2702.

(19) Doffek, C.; Seitz, M. *The radiative lifetime in near-IR luminescent ytterbium cryptates: the key to extremely high quantum yields. Angew. Chem. Int. Ed.* **2015**, *54*, 9719.

(20) Zhang, T.; Zhu, X.; Cheng, C.C.W.; Kwok, W.-M.; Tam, H.-L.; Hao, J.; Kwong, D.W.J.; Wong, W.-K.; Wong, K.-L. Water-soluble mitochondria-specific ytterbium complex with impressive NIR emission. *J. Am. Chem. Soc.* **2011**, *133*, 20120.

(21) Auzel, F.; Goldner, P. Towards rare-earth clustering control in doped glasses. *Opt. Mater.* **2001**, *16*, 93.

(22) Zare, D.; Suffren, Y.; Guénée, L.; Eliseeva, S.V.; Nozary, H.; Aboshyan-Sorgho, L.; Petoud, S.; Hauser, A.; Piguet, C. Smaller than a nanoparticle with the design of discrete polynuclear molecular complexes displaying near-infrared to visible upconversion. *Dalton Trans.* **2015**, *44*, 2529.

(23) Salley, G.M.; Valiente, R.; Güdel, H.U. Phonon-assisted cooperative sensitization of Tb^{3+} in $SrCl_2$: Yb, Tb. *J. Phys.: Condens. Matter* **2002**, *14*, 5461.

(24) Salley, G.M.; Valiente, R.; Güdel, H.U. Cooperative Yb^{3+}–Tb^{3+} dimer excitations and upconversion in $Cs_3Tb_2Br_9$:Yb^{3+}. *Phys. Rev. B*, **2003**, *67*, 134111.

(25) Salley, G.M.; Valiente, R.; Güdel, H.U. Luminescence upconversion mechanisms in Yb^{3+}–Tb^{3+} systems. *J. Lumin.* **2001**, *94-95*, 305.

(26) Abada, S.; Lecointre, A.; Elhabiri, M.; Charbonnière, L.J. Formation of very stable and selective Cu(II) complexes with a non-macrocyclic ligand: can basicity rival pre-organization? *Dalton Trans.* **2010**, *39*, 9055.

(27) Lukes, I.; Kotek, J.; Vojtisek, P.; Hermann, P. Complexes of tetraazacycles bearing methylphosphinic/phosphonic acid pendant arms with copper(II), zinc(II) and lanthanides(III). A comparison with their acetic acid analogues. *Coord. Chem. Rev.* **2001**, *216-217*, 287.

(28) Benetollo, F.; Bombieri, G.; Calabi, L.; Aime, S.; Botta, M. Structural variations across the lanthanide series of macrocyclic DOTA complexes: insights into the design of contrast agents for magnetic resonance imaging. *Inorg. Chem.* **2003**, *42*, 148.

(29) Avecilla, F.; Peters, J.A.; Geraldes, C.F.G.C. X-ray crystal structure of a sodium salt of $[Gd(DOTP)]^{5-}$: implications for its second-sphere relaxivity and the ^{23}Na NMR hyperfine shift effects of $[Tm(DOTP)]^{5-}$. *Eur. J. Inorg. Chem.* **2003**, 4179.

(30) Pellegatti, L.; Zhang, J.; Drahos, B.; Villette, S.; Suzenet, F.; Guillaumet, G.; Petoud, S.; Tóth, E. Pyridine-based lanthanide complexes: towards bimodal agents operating as near infrared luminescent and MRI reporters. *Chem. Commun.* **2008**, 6591.

(31) Abada, S.; Lecointre, A.; Elhabiri, M.; Esteban-Gomez, D.; Platas-Iglesias, C.; Tallec, G.; Mazzanti, M.; Charbonnière, L.J. Highly relaxing gadolinium based MRI contrast agents responsive to Mg^{2+} sensing. *Chem. Commun.* **2012**, *48*, 4085.

(32) Aime, S.; Gianolo, S.; Corpillo, D.; Cavalotti, C.; Palmisano, G.; Sisti, M.; Giovenzana, G.B.; Pagliarin, R. Designing novel contrast agents for magnetic resonance imaging. Synthesis and relaxometric characterization of three gadolinium(III) complexes based on functionalized pyridine-containing macrocyclic ligands. *Helv. Chim. Acta*, **2033**, *86*, 615.

(33) Elhabiri, M.; Abada, S.; Sy, M.; Nonat, A.; Choquet, P.; Esteban-Gomez, D.; Cassino, C.; Platas-Iglesias, C.; Botta, M.; Charbonnière, L.J. Importance of outer-sphere and aggregation phenomena in the relaxation properties of phosphonated gadolinium complexes with potential applications as MRI contrast agents. *Chem. Eur. J.* **2015**, *21*, 6535.

(34) Souri, N.; Tian, P.; Lecointre, A.; lemaire, Z.; Chafaa, S.; Strub, J.-M.; Cianférani, S.; Elhabiri, M.; Platas-Iglesias, C.; Charbonnière, L.J. Step by step assembly of polynuclear lanthanide complexes with a phosphonated bipyridine ligand. *Inorg. Chem.* **2016**, 55, 12962.

(35) Salaam, J.; Tabti, L.; Bahamyirou, S.; Lecointre, A.; Hernandez Alba, O.; Jeannin, O.; Camerel, F.; Cianférani, S.; Bentouhami, E.; Nonat, A.M.; Charbonnière, L.J. Formation of mono- and polynuclear luminescent lanthanide complexes based on the coordination of preorganized phosphonated pyridines. *Inorg. Chem.* **2018,** 57, 6095.

(36) Llunell, M.; Casanova, D.; Cirera, J.; Alemany, P.; Alvarez, S. SHAPE (version 2.1), Barcelona, 2013.

(37) Ruiz-Martinez, A.; Casanova, D.; Alvarez, S. Polyhedral Structures with an Odd Number of Vertices: Nine-Coordinate Metal Compounds. *Chem. Eur. J.*, **2008**, *14*, 1291.

(38) Peters, J. A.; Huskens, J. & Raber, D. J. Lanthanide induced shifts and relaxation rate enhancements. *Prog. Nucl. Magn. Reson. Spectrosc.* **28**, 283-350 (1996).

(39) Aime, S.; Barbero, L.; Botta, M.; Ermondi, G. Determination of metal–proton distances and electronic relaxation times in lanthanide complexes by nuclear magnetic resonance spectroscopy. *J. Chem. Soc., Dalton Trans.* **1992**, 225.

(40) Frisch, M. J.; Trucks, G. W.; Schlegel, H. B.; Scuseria, G. E.; Robb, M. A.; Cheeseman, J. R.; Scalmani, G.; Barone, V.; Mennucci, B.; Petersson, G. A., Nakatsuji,H.; Caricato, M.; Li, X.; Hratchian, H. P.; Izmaylov, A. F.; Bloino, J.; Zheng, G.; Sonnenberg, J. L.; Hada, M.; Ehara, M.; Toyota, K.; Fukuda, R.; Hasegawa, J.; Ishida, M.; Nakajima, T.; Honda, Y.; Kitao, O.; Nakai, H.; Vreven, T.; Montgomery Jr., J.A.; Peralta, J. E.; Ogliaro, F.; Bearpark, M.; Heyd, J. J.; Brothers, E.; Kudin, K. N.; Staroverov, V. N.; Kobayashi, R.; Normand, J.; Raghavachari, K.; Rendell, A.; Burant, J. C. ; Iyengar, S. S.; Tomasi, J.; Cossi, M.; Rega, N.; Millam, J.M.; Klene, M. ; Knox, J. E.; Cross, J. B.; Bakken, V.; Adamo, C.; Jaramillo, J.; Gomperts, R. ; Stratmann, R. E.; Yazyev, O.; Austin, A. J.; Cammi, R.; Pomelli, C.; Ochterski, J. W.; Martin, R. L.; Morokuma, K.; Zakrzewski, V. G.; Voth, G.A.; Salvador, P.; Dannenberg, J. J.; Dapprich, S.; Daniels, A. D.; Farkas, Ö.; Foresman, J. B.; Ortiz, J. V.; Cioslowski, J.; Fox, D.J. Gaussian 09, Revision E.01, Gaussian, Inc.: Wallingford CT, 2009.

(41) Forsberg, J. H.; Delaney, R. M.; Zhao, Q.; Harakas, G.; Chandran, R. Analyzing lanthanide-induced shifts in the NMR spectra of lanthanide(III) complexes derived from 1,4,7,10-tetrakis(N,N-diethylacetamido)-1,4,7,10-tetraazacyclododecane. *Inorg. Chem.* **1995**, *34*, 3705.

(42) Blackburn, O. A.; Routledge, J. D.; Jennings, L. B.; Rees, N. H.; Kenwright, A. M.; Beer, P. D.; Faulkner, S. Substituent effects on fluoride binding by lanthanide complexes of DOTA-tetraamides. *Dalton Trans.* **2016**, *45*, 3070.

(43) Ouali, N.; Bocquet, B.; Rigault, S.; Morgantini, P.-Y.; Weber, J.; Piguet, C. Analysis of paramagnetic NMR spectra of triple-helical lanthanide complexes with 2,6-dipicolinic acid revisited: a new assignment of structural changes and crystal-field effects 25 years later. *Inorg. Chem.* **2002**, *41*, 1436.

(44) Blackburn, O. A.; Chilton. N. F.; Keller, K.; Tait, C. E.; Myers, W. K.; McInnes, E. J. L.; Kenwright, A. M.; Beer, P. D.; Timmel, C. R.; Faulkner, S. Spectroscopic and crystal field consequences of fluoride binding by $[Yb{\cdot}DTMA]^{3+}$ in aqueous solution. *Angew. Chem. Int. Ed.* **2015**, *54*, 10783.

(45) Werts, M.H.V.; Jukes, R.T.F.; Verhoeven, J.W. The emission spectrum and the radiative lifetime of Eu^{3+} in luminescent lanthanide complexes. *Phys. Chem. Chem. Phys.* **2002**, *4*, 1542.

(46) Eliseeva, S.; Bünzli, J.-C.G. Lanthanide luminescence for functional materials and bio-sciences. *Chem. Soc. Rev.* **2010**, *39*, 189.

(47) Pollnau, M.; Gamelin, D.R.; Lüthi, S.R.; Güdel, H.U. Power dependence of upconversion luminescence in lanthanide and transition-metal-ion systems. *Phys. Rev. B: Condens. Matter,* **2000**, *61*, 3337.

(48) Weibel, N.; Charbonnière, L.J.; Guardigli, M.; Roda, A.; Ziessel, R. Engineering of highly luminescent lanthanide tags suitable for protein labeling and time-resolved luminescence imaging. *J. Am. Chem. Soc.* **2004**, *126*, 4888.

(49) Suffren, Y.; Zare, D.; Eliseeva, S. V.; Guénée, L.; Nozary, H.; Lathion, T.; Aboshyan-Sorgho, L.; Petoud, S.; Hauser, A.; Piguet, C. Near-infrared to visible light-upconversion in molecules: from dream to reality. *J. Phys. Chem. C* **2013**, *117*, 26957.

(50) Altomare, A.; Burla, M. C.; Camalli, M.; Cascarano, G. L.; Giacovazzo, C.; Guagliardi, A.; Moliterni, A. G. G.; Polidori, G.; Spagna, R. SIR92 – a program for automatic solution of crystal structures by direct methods. *J. Appl. Crystallogr.* **1999**, *32*, 115.

(51) Sheldrick G. M. Crystal structure refinement with SHELXL. *Acta Cryst. C* **2015**, *71*, 3.

(52) Farrugia L. WinGX and ORTEP for Windows: an update. J. *Appl. Cryst.* **2012**, *45*, 849.

(53) Regueiro-Figueroa, M.; Platas-Iglesias, C. Toward the prediction of water exchange rates in magnetic resonance imaging contrast agents: a density functional theory study. *J. Phys. Chem. A* **2015**, *119*, 6436.

(54) Tao, J. M.; Perdew, J. P.; Staroverov, V. N.; Scuseria, G. E. Climbing the density functional ladder: non-empirical meta-generalized gradient approximation designed for molecules and solids. *Phys. Rev. Lett.* **2003**, *91*, 146401.

(55) Dolg, M.; Stoll, H.; Savin, A.; Preuss, H. Energy-adjusted pseudopotentials for the rare earth elements. *Theor. Chim. Acta* **1989**, *75*, 173.

(56) Tomasi, J.; Mennucci, B.; Cammi, R. Quantum mechanical continuum solvation models. *Chem. Rev.* **2005**, *105*, 2999.

Table Of Content